NACA

RESEARCH MEMORANDUM

EXPERIMENTAL AND THEORETICAL STUDY OF THE INTERFERENCE

AT LOW SPEED BETWEEN SLENDER BODIES

AND TRIANGULAR WINGS

By Edward J. Hopkins and Hubert C. Carel

Ames Aeronautical Laboratory
Moffett Field, Calif.

AFMDC
TECHNICAL LIBRARY
AFL 2311

NATIONAL ADVISORY COMMITTEE
FOR AERONAUTICS
WASHINGTON
May 6, 1953

National Aeronautics and
Space Administration

Langley Research Center
Hampton, Virginia
23665

NAS/

JUN 1 6 1983

Reply to Attn of   139A

TO: Distribution

FROM: 180A/Security Classification Officer

SUBJECT: Authority to Declassify NACA/NASA Documents Dated Prior to
          January 1, 1960

          (informal, correspondence)

Effective this date, all material classified by this Center prior to
January 1, 1960, is declassified. This action does not include material
derivatively classified at the Center upon instructions from other Agencies.

Immediate re-marking is not required; however, until material is re-marked by
lining through the classification and annotating with the following statement,
it must continue to be protected as if classified:

    "Declassified by authority of LaRC Security Classification Officer (SCO)
    letter dated June 16, 1983," and the signature of person performing the
    re-marking.

If re-marking a large amount of material is desirable, but unduly burdensome,
custodians may follow the instructions contained in NHB 1640.4, subpart F,
section 1203.604, paragraph (h).

This declassification action complements earlier actions by the National
Archives and Records Service (NARS) and by the NASA Security Classification
Officer (SCO). In Declassification Review Program 807008, NARS declassified
the Center's "Research Authorization" files, which contain reports, Research
Authorizations, correspondence, photographs, and other documentation.
Earlier, in a 1971 letter, the NASA SCO declassified all NACA/NASA formal
series documents with the exception of the following reports, which must
remain classified:

Document No.	First Author
E-51A30	Nagey
E-53G20	Francisco
E-53G21	Johnson
E-53K18	Spooner
SL-54J21a	Westphal
E-55C16	Fox
E-56H23a	Himmel

JUN 2 3 1983

NATIONAL ADVISORY COMMITTEE FOR AERONAUTICS

RESEARCH MEMORANDUM

EXPERIMENTAL AND THEORETICAL STUDY OF THE INTERFERENCE

AT LOW SPEED BETWEEN SLENDER BODIES

AND TRIANGULAR WINGS

By Edward J. Hopkins and Hubert C. Carel

SUMMARY

The aerodynamic characteristics of several wing-fuselage combinations were measured at a Mach number of 0.25. Each combination consisted of a triangular wing with an aspect ratio of 2.0 and a body of revolution having a fineness ratio of 12.5. The ratios of maximum body diameter to wing span were 0.196, 0.259, 0.343, and 0.500. The measured forces and moments are compared with the predicted values for each of the wing-body combinations and for the wings in the presence of the bodies.

The forces and moments on the wings in the presence of the bodies were, in general, predicted satisfactorily by the Weissinger method. In order to obtain good agreement with experiment for the case of a variable angle of attack and a fixed angle of wing incidence, it was necessary to include in the calculations the velocities which are induced by the body. The Lennertz method gave a good estimate of the forces carried over the body.

INTRODUCTION

The importance of including the forces and moments mutually induced by a wing and a body in theoretical analyses of combinations having relatively large bodies is indicated in reference 1. Good agreement between the experimental and theoretical results is shown therein for an unswept wing (aspect ratio 3.0) combined with a body of revolution for ratios of body diameter to wing span of 0.196, 0.259, and 0.343. A simple procedure is presented in reference 1 for calculating the aerodynamic forces and moments of wing-body combinations, considering the

velocities mutually induced by the wings and bodies and employing the methods of references 2, 3, 4, and 5.

The research reported in reference 1 has been extended to include combinations of triangular wings having an aspect ratio of 2 and bodies of revolution. The aerodynamic forces and moments on the triangular wings in the presence of the bodies and on the wing-body combinations have been measured for ratios of body diameter to wing span of 0.196, 0.259, 0.343, and 0.500. Comparisons are presented herein between the results predicted by the method given in reference 1 and the measured results for each of the triangular wings combined with the bodies and for the triangular wings in the presence of the bodies.

NOTATION

C_b bending-moment coefficient, $\dfrac{4B}{qSb}$

C_L lift coefficient, $\dfrac{\text{lift}}{qS}$

C_D drag coefficient, $\dfrac{\text{drag}}{qS}$

C_m pitching-moment coefficient, $\dfrac{M}{qS\bar{c}}$

C_N normal-force coefficient, $\dfrac{N}{qS}$

b   wing span

B   bending moment of wing about the body longitudinal axis (positive for clockwise direction looking upstream)

c   local wing chord

$\bar{c}$ mean aerodynamic chord, $\dfrac{\int_{-b/2}^{b/2} c^2\,dy}{\int_{-b/2}^{b/2} c\,dy}$

c_r wing root chord on the longitudinal body axis

d   maximum diameter of body

d/b ratio of maximum body diameter to wing span

i_w angle of wing incidence relative to body axis (positive with wing
        trailing edge down)

l body length

L/D lift-to-drag ratio, $\dfrac{C_L}{C_D}$

M pitching moment about the lateral axis passing through the 0.25 $\bar{c}$
        point

N force normal to the body axis

q free-stream dynamic pressure

S total wing area

x longitudinal distance from 0.25 $\bar{c}$ to aerodynamic center (positive
        for distances ahead of 0.25 $\bar{c}$)

y lateral distance from longitudinal axis of body

α angle of attack

$\dfrac{x}{\bar{c}}$ location of aerodynamic center, $\left(\dfrac{dC_m/di_w}{dC_N/di_w}\right)_{\alpha=0^\circ}$ or $\left(\dfrac{dC_m/d\alpha}{dC_N/d\alpha}\right)_{i_w=0^\circ}$

η spanwise location of center of pressure, $\left(\dfrac{dC_b/di_w}{dC_N/di_w}\right)_{\alpha=0^\circ}$

        or $\left(\dfrac{dC_b/d\alpha}{dC_N/d\alpha}\right)_{i_w=0}$

MODEL DESCRIPTION

Each of three geometrically similar triangular wings was combined
separately with the medium-sized body tested in reference 1, with result-
ing ratios of maximum body diameter to wing span of 0.259, 0.343, and
0.500. The largest of these triangular wings was also combined with the
smallest body tested in reference 1 to give a diameter-to-span ratio
of 0.196. Sketches and dimensional data for each of the combinations

are presented in figure 1. For the tests in which the angle of wing incidence was varied, the wing panels were rotated about a lateral axis passing through moment centers shown in figure 1. Photographs of each of the wing-body combinations are presented in figure 2.

Each of the wings had an aspect ratio of 2.0, a taper ratio of zero, a leading-edge sweepback of 63.43°, and the NACA 0005 profile (modified with straight sides near the wing trailing edge) in vertical planes parallel to the wing root chords. The coordinates for this profile are given in table I.

Some tests were conducted with dorsal fins, made of 1/4-inch pressed board, on top of the wing-body combination with $d/b = 0.500$. (See fig. 3.) The vertical height of the dorsal fins was equal to the body radius at each longitudinal station. One dorsal fin extended over the full length of the body, the other extended over only the rear half of the body.

TEST PROCEDURE

The tests were conducted in one of the Ames 7- by 10-foot wind tunnels at a dynamic pressure of 90 pounds per square foot. The Mach number was 0.25 and the Reynolds numbers (based on the mean aerodynamic chord of each wing) were 3.94, 3.94, 2.98, and 2.05 million for the models having diameter-to-span ratios of 0.196, 0.259, 0.343, and 0.500, respectively. Measurements were made of the normal-force, pitching-moment, and bending-moment characteristics of the wings in the presence of the bodies and of the pitching-moment, lift, and drag characteristics of the wing-body combinations. The forces and moments were measured on the wings in the presence of the bodies with the wings at angles of incidence relative to the body axis of 0°, 2°, 4°, 6°, 8°, and 10°. The forces and moments were also measured for each of the combinations with the wings rigidly attached to the bodies at angles of wing incidence of 0°, 6°, and 10°.

The six-component balance system of the wind tunnel was used to measure the forces and moments on the wing-body combinations. For the measurements of the forces and moments on the wings in the presence of the bodies, the left wing panels were supported from within the bodies by a three-component strain-gage system. Data were taken for the wing-body combinations throughout an angle-of-attack range from 0° to 28°. The angle-of-attack range for the wing in the presence of the body was from 0° to 20°, because deflection of the strain gages would allow the wing to touch the body at higher angles of attack.

With the wings mounted on the strain gages, the following portions of the wing-body intersections were sealed.

$\dfrac{d}{b}$	Portion sealed, % c
0.196	15 to 71
.259	0 to 61
.343	0 to 69
.500	0 to 82

The seals consisted of thin rubber tubes filled with air which was main-tained at a constant pressure throughout the angle-of-attack range. With the wing incidence 0°, a gap not wider than three-sixteenths inch existed between each of the wings and the bodies over that part of the intersection which was unsealed. As the angle of wing incidence was increased up to 10° these gaps progressively became larger. Photographs of the gaps between the wings and the bodies with a wing incidence of 10° are shown in figure 4.

For the tests of the wing-body combinations with the wings rigidly attached to the bodies, measurements were made with the gaps at the wing-body intersections sealed and unsealed.

CORRECTIONS

The aerodynamic effects of the model support struts (strut tares) were determined by means of an image-strut system. The strut tares measured with the wing incidence 0° were also applied to the data with the wing incidence other than 0°.

The experimental data were corrected for the effects of the wind-tunnel walls by the method of reference 6. Neither sweep nor body effects were taken into account in applying these corrections. The mag-nitudes of the effects of sweep and of the bodies on the corrections were estimated to be within the accuracy of the experimental results. The angle of attack and the drag coefficients were corrected as follows:

$$\alpha = \alpha_u + K_1 \, C_{L_u}$$

$$C_D = C_{D_u} + K_2 \left(C_{L_u} \right)^2$$

where the subscript u denotes the uncorrected values. The constants
K_1 and K_2 are given below for each model.

d/b	0.500	0.343	0.250	0.196
K_1	0.186	0.415	0.770	0.770
K_2	.00277	.00576	.00996	.00996

With the wings mounted on the strain gages, the change in the angle
of wing incidence due to the deflection of the gages by aerodynamic
loads was calculated from stress considerations and checked during the
calibration of the strain gages. All the data for the wings in the
presence of the bodies have been corrected for this change in incidence.
The magnitude of this correction was not greater than $0.6°$ for any of
the wing-body combinations. To arrive at curves for constant angles of
incidence, it was necessary to crossplot the data; therefore, no experi-
mental points appear in the figures containing the data for the wings
in the presence of the bodies.

RESULTS AND DISCUSSION

In the discussion that follows, the experimental results are
presented for the wings in the presence of the bodies and for the wing-
body combinations. The experimental results are compared with the
theoretical results for each model. The procedure followed in calculat-
ing the forces and moments is described briefly herein and in more
detail in reference 1.

Wings in the Presence of the Bodies

The measured normal-force, pitching-moment, and bending-moment
coefficients as functions of angle of attack are presented in fig-
ures 5(a), 5(b), and 5(c) for constant angles of wing incidence. The
results from cross plotting these coefficients for an angle of attack
of $0°$ are presented as functions of wing incidence in figures 5(d), 5(e),
and 5(f).

For variable wing incidence ($\alpha = 0°$), the theoretical normal-force
curves in figure 5(d) were calculated by the Weissinger method (ref. 2)
with the neglect of any reflected induced forces from the body. The
normal-force coefficients C_{N_1} based upon the total wing area were cal-
culated by the following equation:

$$C_{N_1} = \left(1 - \frac{d}{b}\right)^2 \left(\frac{i_w}{\cos i_w}\right)\left(\frac{dC_L}{di_w}\right) \tag{1}$$

where it is assumed that dC_L/di_w is the Weissinger lift-curve slope given in reference 2[1] and $C_L = C_N \cos i_w$. The close agreement between the experimental and theoretical normal-force-curve slopes in figure 5(d) indicates that the bodies induced a negligible amount of normal force on the wings when the body angle of attack was $0°$. Throughout the figures it will be noted that some of the experimental curves do not pass through zero at $\alpha = i_w = 0°$ as would be expected for the symmetrical models. The complete explanation for this displacement is unknown, but it may be attributed largely to inaccuracies in initial settings of i_w and α, to slight asymmetry of the wings and bodies, or to inaccurate determination of tares. The comparisons between the experimental and theoretical force and moment coefficients will therefore be made on the basis of the slopes of the curves.

The theoretical values of the pitching-moment and bending-moment coefficients in figures 5(e) and 5(f), for variable wing incidence ($\alpha = 0°$), were calculated by assuming the normal force to act at the position given by the Weissinger method (ref. 2). The equations for calculating these coefficients for triangular wings are

$$C_m = \left[\frac{3}{4} - \frac{9}{8}(1-\eta_1)\left(1 - \frac{d}{b}\right)\right] C_{N_1} \tag{2}$$

$$C_b = \left[\eta_1\left(1 - \frac{d}{b}\right) + \frac{d}{b}\right] C_{N_1} \tag{3}$$

where η_1 is the spanwise center-of-pressure position given in reference 2. As shown in figure 5(e) the predicted pitching moments are low by as much as 20 percent for the smallest d/b ratios, but were essentially correct for the largest diameter-to-span ratios. The experimental bending-moment coefficients are in good agreement with the predicted values for all the combinations presented in figure 5(f).

For variable angle of attack ($i_w = 0°$), the forces induced by the body on the wing must be accounted for in the calculations to realize close agreement with the experimental results for wing-body combinations having large body diameters relative to wing span. (See ref. 1.)

---

[1]For any wing-body combination employing a triangular wing, the aspect ratio based upon the exposed area and span has the same value as the aspect ratio based upon the total area and span.

These induced forces were calculated by the Weissinger method, using the body-induced flow angles given by potential-flow theory for bodies in the manner illustrated in reference 1. These induced normal-force coefficients C_{N_2} were added to the coefficients C_{N_1} calculated by equation (1) so that the normal-force coefficient becomes $C_N = C_{N_1} + C_{N_2}$. The results, shown in figure 5(a), of following this procedure indicate that the predicted normal forces were of the proper magnitude for the smallest diameter-to-span ratio, low for the two largest diameter-to-span ratios, but considerably low for the combination with $D/b = 0.259$. The reason for the larger difference between experiment and theory for the latter combination is unknown.

For variable angle of attack ($i_w = 0°$), the pitching- and bending-moment coefficients were also calculated from equations (2) and (3) but by using a different spanwise location of the center of pressure η_3, derived by considering the location and magnitude of the force induced by the body. The value of η_3 was calculated from the following equation:

$$\eta_3 = \frac{\left(C_{N_1}\right)\left(\eta_1\right) + \left(C_{N_2}\right)\left(\eta_2\right)}{C_{N_1} + C_{N_2}}$$

where C_{N_2} denotes the normal-force coefficient induced by the body (based on the total wing area), and η_2 is the spanwise location of the center of pressure of the normal force induced by the body, measured from the wing-body intersection (see ref. 1).

According to the results presented in figures 5(b) and 5(c), this procedure gave about the proper magnitudes of the pitching and bending moments for the two largest diameter-to-span ratios but underestimated the pitching and bending moments for the two smallest diameter-to-span ratios.

The measured and predicted effects of changes in the relative size of the wing on the location of the aerodynamic center and spanwise location of the center of pressure are shown in figure 6. The experimental points for the wing alone ($d/b = 0$) are from reference 7. The comparison presented in figure 6 indicates that the theory, in general, gives the proper variation of the locations with diameter-to-span ratio. The experimental scatter shown in figure 6 might be considered indicative of the accuracy of the experimental results.

Wing-Body Combinations

The span load distribution on wings having low aspect ratios is approximately elliptical. For this reason the calculations made by Lennertz in reference 5 for an idealized wing-body combination with minimum induced drag were used for estimating the amount of load carried over the bodies of the present investigation. The results of his calculations for wing-load carry-over as a function of diameter-to-span ratio are shown in figure 7. The experimental points shown in figure 7 were computed from the expression

$$\frac{(dC_N/di_w)_{wing\ +\ body}}{(dC_N/di_w)_{wing\ in\ presence\ of\ body}}$$

for which the angle of attack is 0°, since it was not possible to isolate from the experimental results the amount of load carried on the body in front of and behind the wing with the body inclined. The experimental values computed by this method are within 6 percent of those given by Lennertz.

The experimental normal-force and pitching-moment characteristics for the various wing-body combinations with the gaps sealed and unsealed are presented in figure 8. (See Test Procedure for description of gaps.) The results indicate that the seals had a small or negligible effect with an angle of incidence of 0°, but the seals generally increased the normal force and the longitudinal stability at the higher angles of incidence for the smallest diameter-to-span ratios. At an angle of incidence of 0°, data were taken for the diameter-to-span ratio of 0.5 only with the gaps sealed. The incremental normal force produced by a wing-incidence change decreased considerably at the higher angles of attack as the diameter-to-span ratio became large. For the diameter-to-span ratio of 0.5, a wing incidence change was relatively ineffective in increasing the normal force at angles of attack above about 20°.

For variable incidence ($\alpha = 0^\circ$), the theoretical results shown in figures 8(e) and 8(f) for the combinations were calculated by multiplying the normal-force and pitching-moment coefficients computed from equations (1) and (2) by the Lennertz carry-over factor in figure 7. This method neglects any mutually reflected effects from the wing and the body and assumes that the chordwise position of load on the body is identical to the position of the load on the wing in the presence of the body. Comparison between experiment and theory in figure 8(e) indicates

that this method gives the proper magnitude of the normal force for all the combinations. However, as shown in figure 8(f), the theory tends to underestimate the pitching moments at the higher angles of incidence, especially for the larger diameter-to-span ratios. It is believed that these discrepancies are caused primarily by neglect of the flow induced by the wing over the body. Flow observations by means of tufts mounted on the combination with $d/b = 0.343$ indicated that the downwash angles behind the wing are greater than the upwash angles in front of the wing. With these induced angles accounted for in the calculations, more negative pitching moments would have been predicted than those presented in figure 8(f).

The theoretical results presented for the wing-body combinations in figures 8(a), 8(b), 8(c), and 8(d) with variable angle of attack ($i_w = 0°$), were calculated by adding the forces and moments for the wing in the presence of the body (with the body induced effects included) times the Lennertz carry-over factor to the forces and moments on the body as given by potential theory. The forces on the body behind the wing were considered zero because the flow leaves the trailing edge of a low-aspect-ratio wing nearly parallel to the mean line of the wing. On the assumption that potential flow exists, it can be shown easily that the lift on the body ahead of the wing depends only upon the flow angle and the body cross-sectional area at the intersection of the wing leading edge and the body surface (e.g., ref. 4). For the highly swept wings, it makes little difference in the final calculated results whether or not the velocities induced by the bound vortex line are considered. In view of this fact, the angles induced by the bound vortex were neglected in the calculations, and the flow angles at the intersection of the wing leading edge and the body surface were assumed to be equal to the angle of attack. This procedure differs therefore from the procedure given in the appendix of reference 1 in which these induced angles were accounted for in the calculations for unswept wings. From the derivations given in reference 8 the normal-force and pitching-moment slopes for the body ahead of the intersection of the wing leading edge with the body surface, with potential flow assumed, are:

$$C_{N_\alpha} = \left(\frac{2}{57.3}\right)\left(\frac{S_1}{S}\right)$$

$$C_{m_\alpha} = \left(\frac{2}{57.3}\right)\left[\frac{(Vol)_1 - S_1(x_m)}{S\bar{c}}\right]$$

with the assumption that $\cos\alpha \cong 1.0$.

The symbols not defined hereinbefore are:

S_1 cross-sectional area of the body at the intersection of the
wing leading edge and the body

$(Vol)_1$ volume of the body from the body nose up to the point at which
the wing leading edge intersects the body

x_m longitudinal distance from the moment center to the intersection
of the wing leading edge with the body (positive for moment
centers ahead of this intersection point)

Good agreement is indicated in figures 8(a) to 8(d) between the
experimental and predicted normal-force and pitching-moment slopes at
the low angles of attack, except for the largest diameter-to-span ratio.
It can be concluded that the lack of agreement for this combination is
a result of an inadequate analysis of the forces and moments on the
body in the presence of the wing. At the higher angles of attack both
the normal-force and pitching-moment results indicate, particularly for
the combinations with the smaller wings, a positive force acting behind
the moment center, possibly a normal force produced by the viscosity of
the fluid. This suggestion of a normal force due to viscosity effects
is further substantiated by the gradually increased curvature of the
normal-force curves as the body becomes larger relative to the wing.
This force would theoretically be proportional to the square of the
angle of attack. The inclusion of this additional normal force in the
calculations would also improve the agreement between the experimental
and predicted pitching-moment coefficients at the higher angles of
attack.

The aerodynamic-center locations for the combinations are presented
in figure 9 as a function of diameter-to-span ratio. For variable angle
of attack ($i_w = 0^\circ$), the predicted variations of the locations with
diameter-to-span ratio are in general agreement with the experimental
variation. However, with variable angle of incidence ($\alpha = 0^\circ$) the pre-
dicted locations are forward of the measured locations. As suggested
previously, this discrepancy is probably attributable to the neglect of
the flow induced by the wings on the bodies.

The drag characteristics of all the wing-body combinations ($i_w = 0^\circ$)
are shown in figure 10. Sealing the small gaps between the wings and
the bodies had the detrimental effect of decreasing slightly the maximum
lift-to-drag ratios. The combinations with the smaller wings were the
least efficient combinations as evidenced by the lower lift-to-drag
ratios.

Dorsal Fins

During the course of the investigation, a large increase in static longitudinal stability was noted for the largest diameter-to-span ratio at angles of attack above 22°. (See fig. 8(d).) It was reasoned that a more linear pitching-moment curve would result if the normal forces near the rear of the body could be reduced at the high angles of attack. Unpublished results for a circular cylinder indicate that a plate alined in the free-stream direction and attached on the lee of the cylinder reduces the cross force at subcritical Reynolds numbers. Consequently, dorsal fins having two different lengths were tested on the upper surface of the fuselage with the smallest wing. One dorsal fin extended over the length of the fuselage and the other covered the rear 50 percent of the length of the fuselage. The experimental results are presented in figure 11. The dorsal fins made the pitching-moment curve more linear at the higher angles of attack, but did not greatly affect the data at the lower angles of attack. The drag results presented in figure 11(b) show that either dorsal fin increased the total drag at all normal-force coefficients.

CONCLUSIONS

The results of tests at a Mach number of 0.25 of several combinations of slender bodies and triangular wings which had ratios of maximum diameter-to-wing span, d/b of 0.196, 0.259, 0.343, and 0.500, indicate the following:

Wings in Presence of Bodies

1. For a variable wing incidence and an angle of attack of 0°, the normal forces and bending moments were satisfactorily predicted by use of the Weissinger method, with the neglect of any mutually induced effects between the wings and the bodies. The pitching moments were accurately predicted for the two smallest wings but were predicted up to 20 percent below the measured values for the largest wing relative to the fuselage.

2. For a variable angle of attack and an angle of incidence of 0°, the predicted normal forces, which included those forces induced by the bodies, were of the proper magnitude for $d/b = 0.196$, low for $d/b = 0.343$ and 0.500, but considerably low for $d/b = 0.259$. The pitching and bending moments were correctly estimated for $d/b = 0.343$ and 0.500; but the pitching and bending moments were underestimated for $d/b = 0.196$ and 0.259.

3. The theory gives, in general, the proper variations of the location of the aerodynamic center and the spanwise location of the center of pressure with relative wing size.

Wing-Body Combinations

1. For a variable wing incidence and an angle of attack of 0°, the normal forces were satisfactorily predicted by applying the Lennertz carry-over factor to the predicted forces for the wing in the presence of the bodies. The theory gave the proper magnitude of the pitching moments for $d/b = 0.196$ and 0.259, but underestimated considerably the values for $d/b = 0.343$ and 0.500. These low estimates are believed to be a result of neglecting the flow induced by the wing over the body.

2. For a variable angle of attack and a wing incidence of 0°, good agreement with the experimental forces and moments was obtained, except for the combination with the smallest wing, at low angles of attack by including the forces acting on the forward part of the bodies, as given by potential-flow considerations, in the calculations and by applying the Lennertz carry-over factor to the predicted forces for the wing in the presence of the bodies. For the smallest wing, poor agreement was obtained; this may be attributable to inadequacy of the analysis of the forces on the body in the presence of the wing.

3. For a variable angle of attack and an angle of incidence of 0°, theory gave the proper variation of the aerodynamic-center location with relative wing size. For a variable angle of incidence and an angle of attack of 0°, theory gave aerodynamic centers considerably forward of the measured locations. The discrepancies in this case were probably caused by neglect of the flow induced by the wing on the body in the calculations.

4. The incremental normal forces produced by a wing-incidence change decreased considerably at the high angles of attack as wing size decreased relative to the fuselage.

5. Dorsal fins on the body with the smallest wing eliminated the large increase in longitudinal stability above an angle of attack of 22°.

Ames Aeronautical Laboratory
    National Advisory Committee for Aeronautics
        Moffett Field, Calif.

REFERENCES

1. Hopkins, Edward J., and Carel, Hubert C.: Experimental and
   Theoretical Study of the Effect of Body Size on the Aerodynamic
   Characteristics of an Aspect Ratio 3.0 Wing-Body Combination.
   NACA RM A51G24, 1951.

2. DeYoung, John, and Harper, Charles W.: Theoretical Symmetric Span
   Loading at Subsonic Speeds for Wings Having Arbitrary Plan Form.
   NACA Rep. 921, 1948.

3. DeYoung, John: Theoretical Symmetric Span Loading Due to Flap
   Deflection for Wings of Arbitrary Plan Form at Subsonic Speeds.
   NACA Rep. 1071, 1952. (Supersedes NACA TN 2278)

4. Multhopp, H.: Aerodynamics of the Fuselage. NACA TM 1036, 1942.

5. Lennertz, J.: Influence of the Airplane Body on the Wings.
   Vol. IV of Aerodynamic Theory, div. K, ch. III, sec. 1,
   W. F. Durand, ed., Julius Springer (Berlin), 1935, pp. 152-157.

6. Swanson, Robert S., and Gillis, Clarence L.: Wind-Tunnel Calibra-
   tion and Correction Procedures for Three-Dimensional Models.
   AAR L4E31 (WRL-1) October 1944. NACA WR L-1, 1944. (Supersedes
   NACA AAR L4E31)

7. Wick, Bradford H.: Chordwise and Spanwise Loadings Measured at Low
   Speed on a Triangular Wing Having an Aspect Ratio of Two and an
   NACA 0012 Airfoil Section. NACA TN 1650, 1948.

8. Allen, H. Julian: Estimation of the Forces and Moments Acting on
   Inclined Bodies of Revolution of High Fineness Ratio. NACA
   RM A9I26, 1949.

TABLE I.- COORDINATES FOR THE WING SECTIONS
(MODIFIED NACA 0005)

Station (percent chord)	Ordinate (percent chord)
0	0
1.25	.79
2.50	1.09
5.00	1.48
7.50	1.75
10.00	1.95
15.00	2.23
20.00	2.39
25.00	2.48
30.00	2.50
40.00	2.42
50.00	2.21
60.00	1.90
67.00	1.65
70.00	1.50
80.00	1.00
90.00	.50
100.00	0
L.E. radius: 0.28 percent c	

Note: Moment centers at 0.25c̄ or c_r/2.
All dimensions in inches.
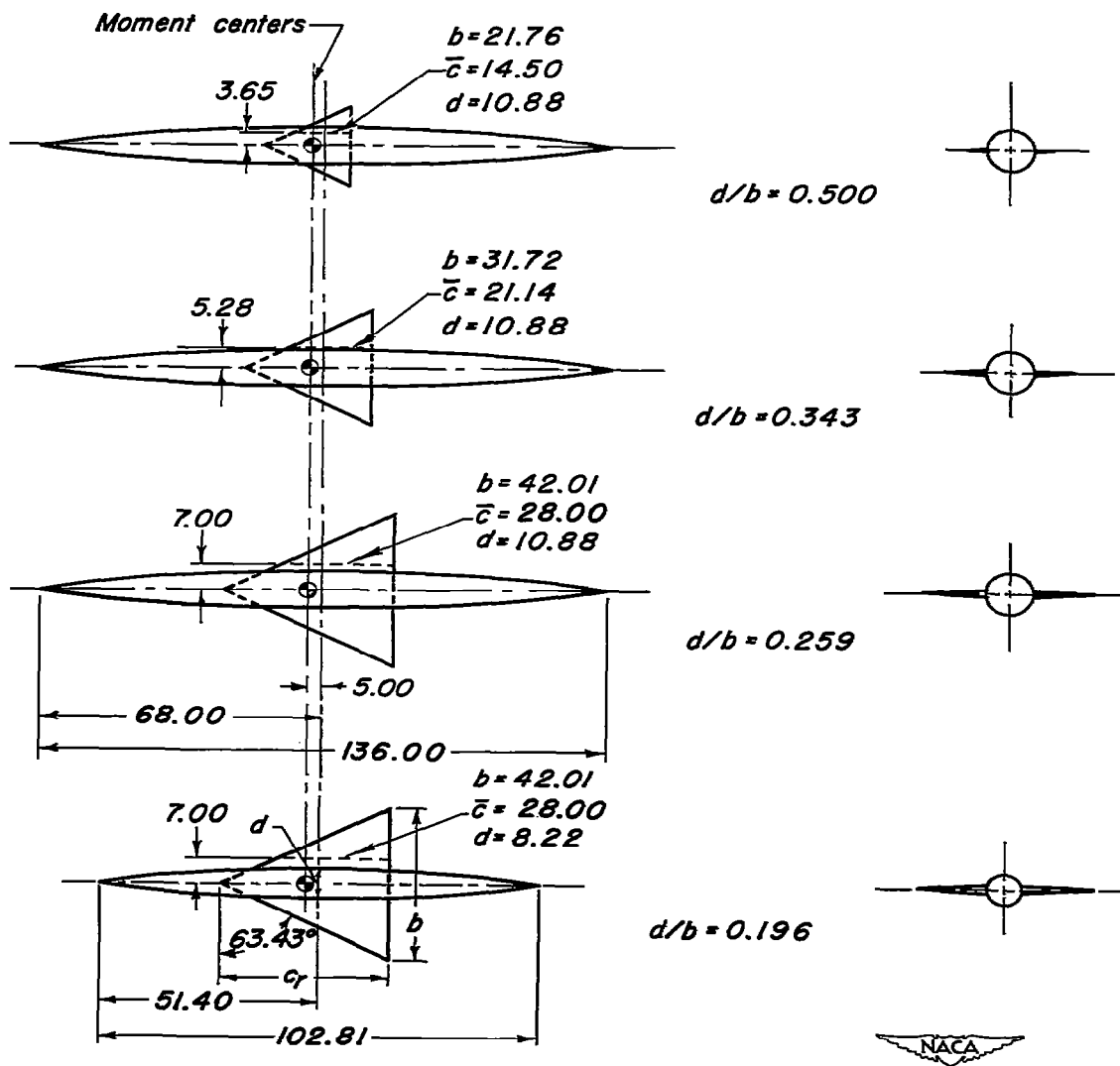
Figure 1.— Model dimensions.

(a) $d/b = 0.196$ (b) $d/b = 0.259$

Figure 2.— Triangular-wing-body combinations mounted in one of the
Ames 7- by 10-foot wind tunnels.

(c) d/b = 0.343
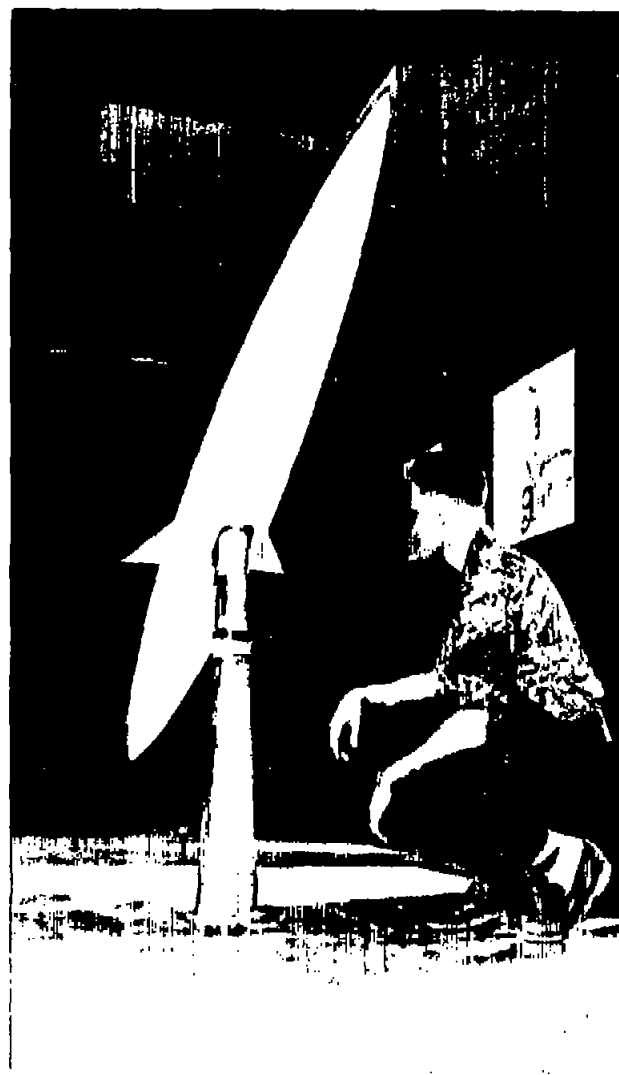
(d) d/b = 0.500

Figure 2.— Concluded.

Figure 3.— Triangular—wing—body combination (d/b = 0.500) with full—
length dorsal fin.

(a) d/b = 0.196
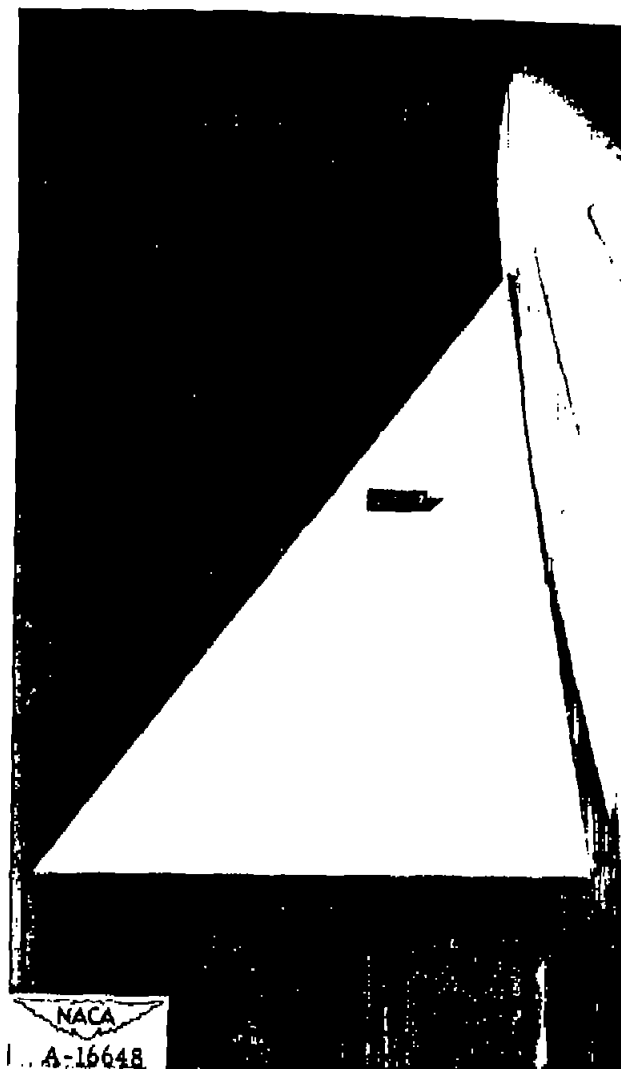
(b) d/b = 0.259

Figure 4.— Gaps between triangular wings and bodies with the wing angle of incidence of 10°.
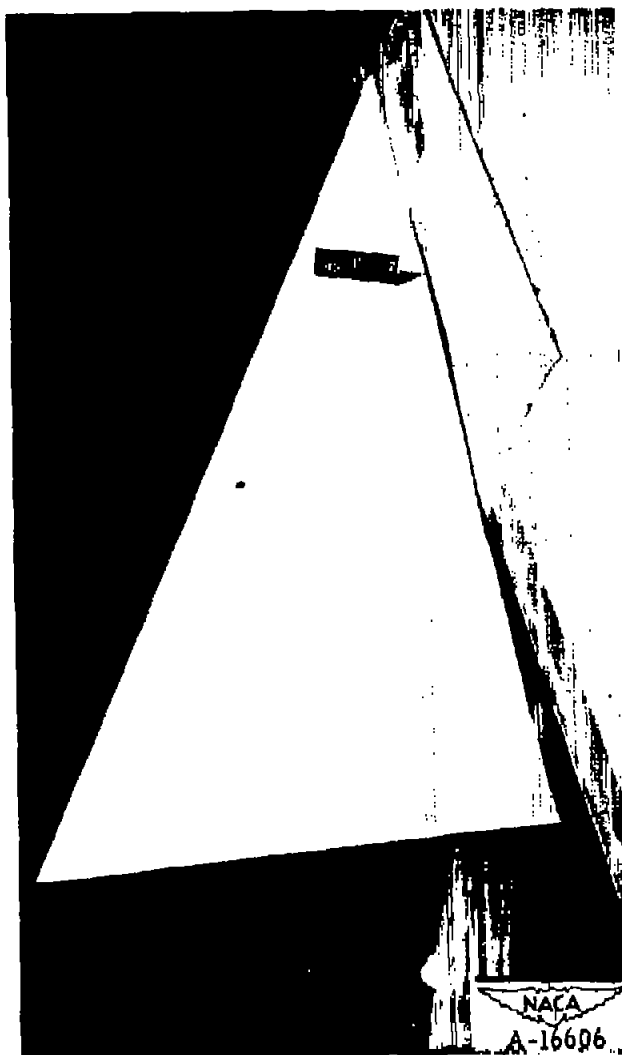
(c) d/b = 0.343
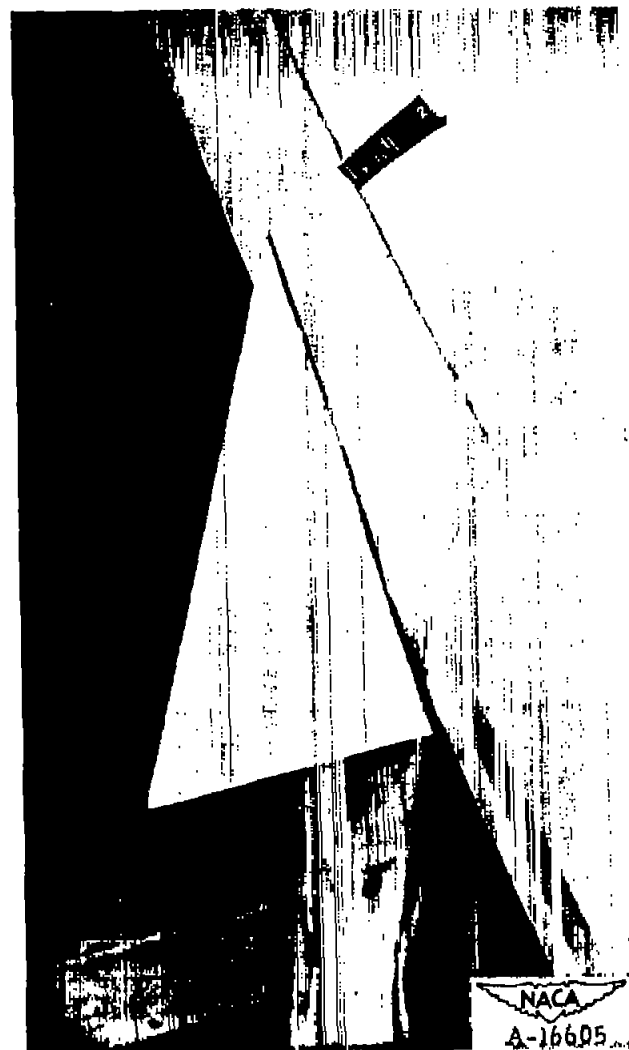
(d) d/b = 0.500

Figure 4.— Concluded.
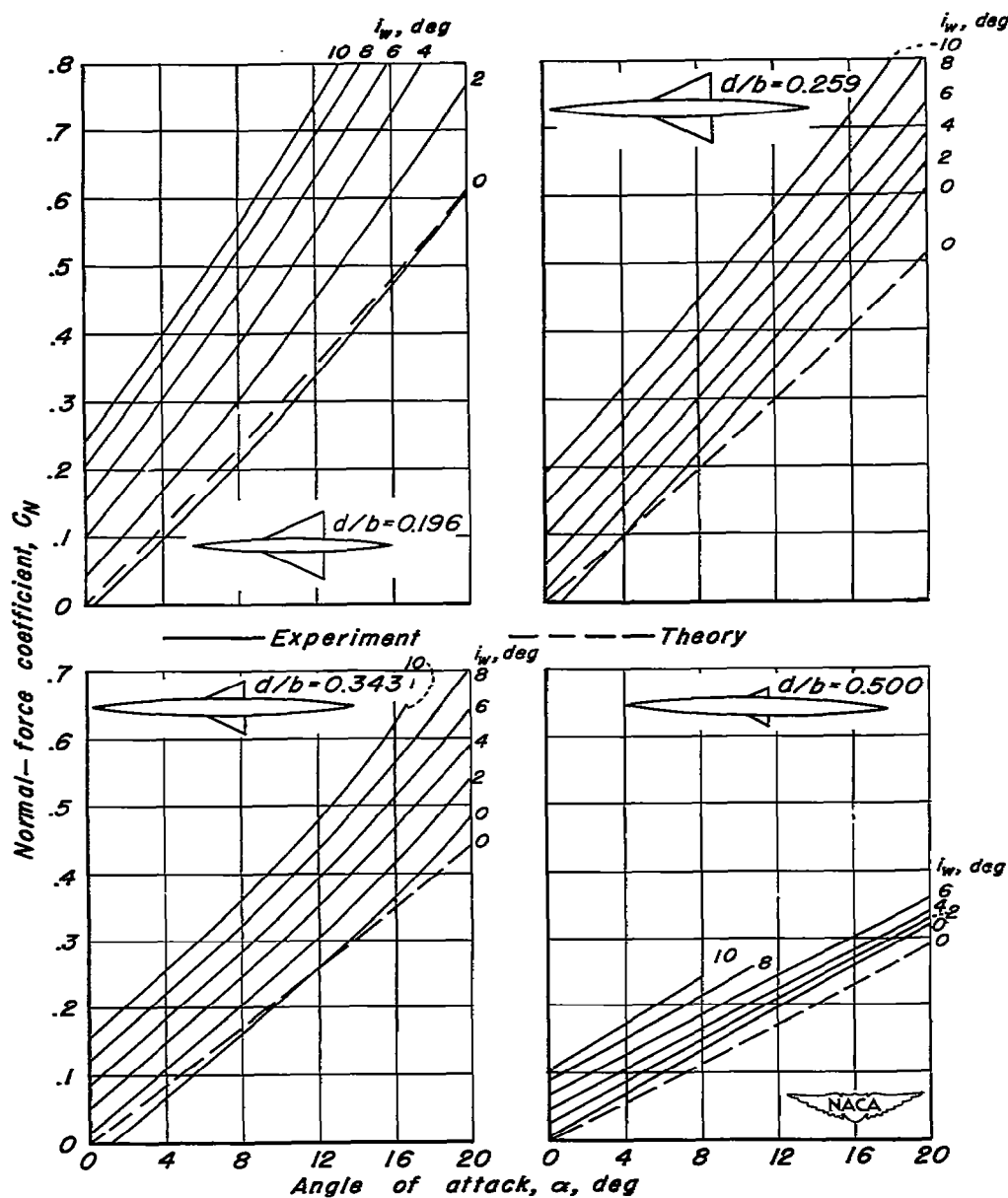
(a) C_N vs α

Figure 5.— Comparison between experimental and theoretical aerodynamic char-acteristics of the wings in the presence of the bodies.
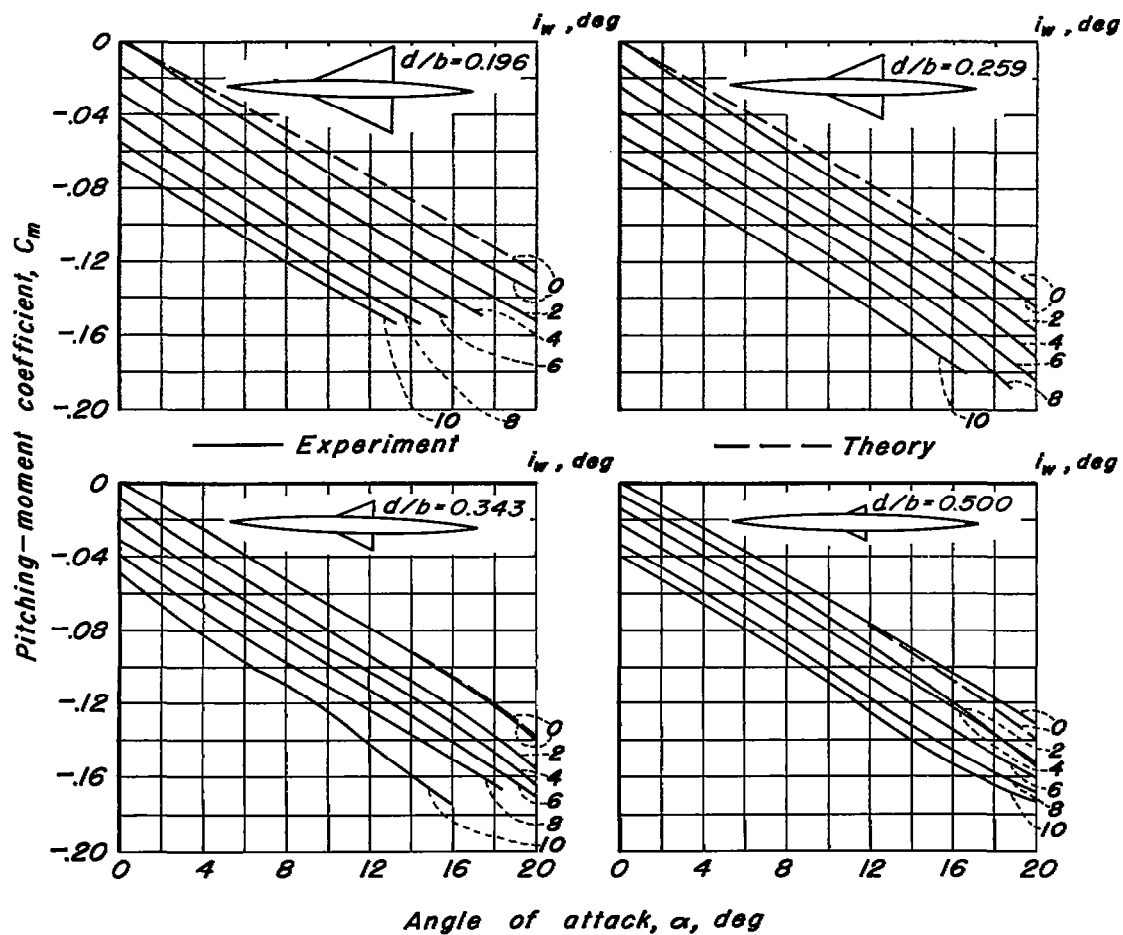
(b) C_m vs α

Figure 5.— Continued.
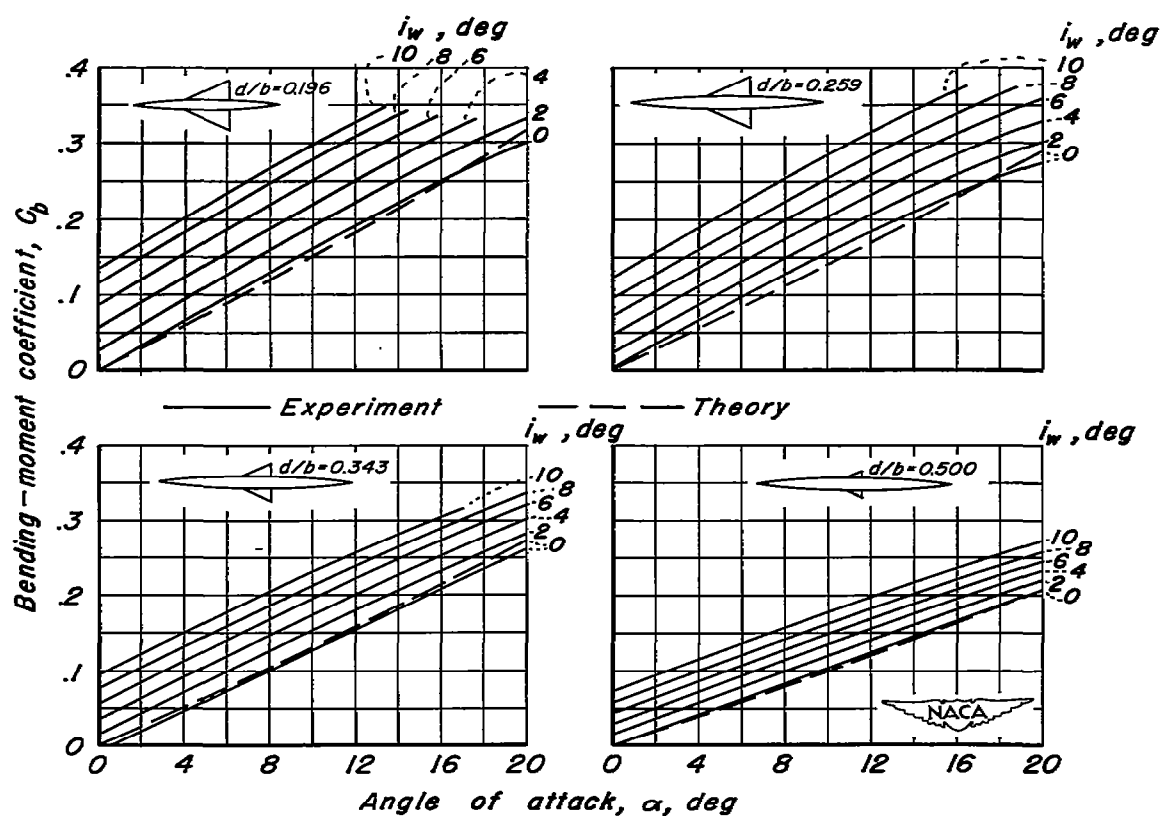
(c) C_b vs α
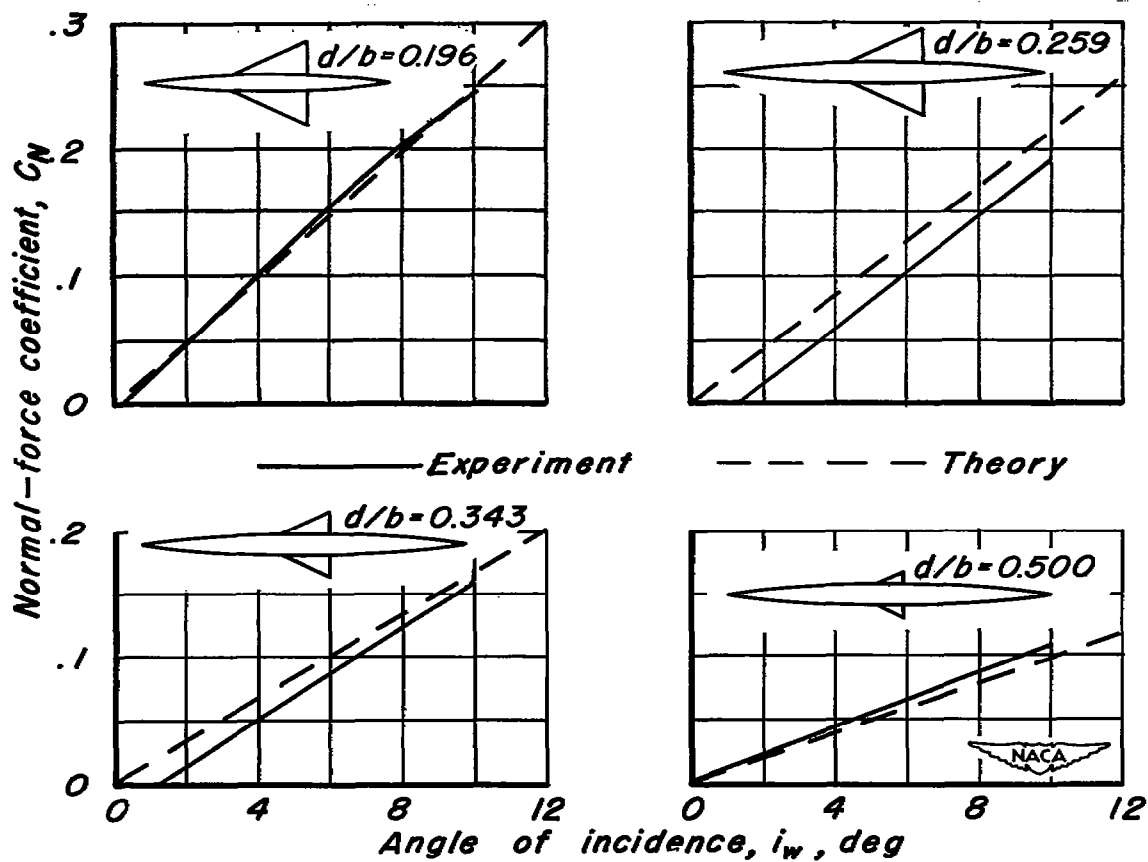
Figure 5.— Continued.

(d) C_N vs i_w, $\alpha = 0°$

Figure 5.— Continued.
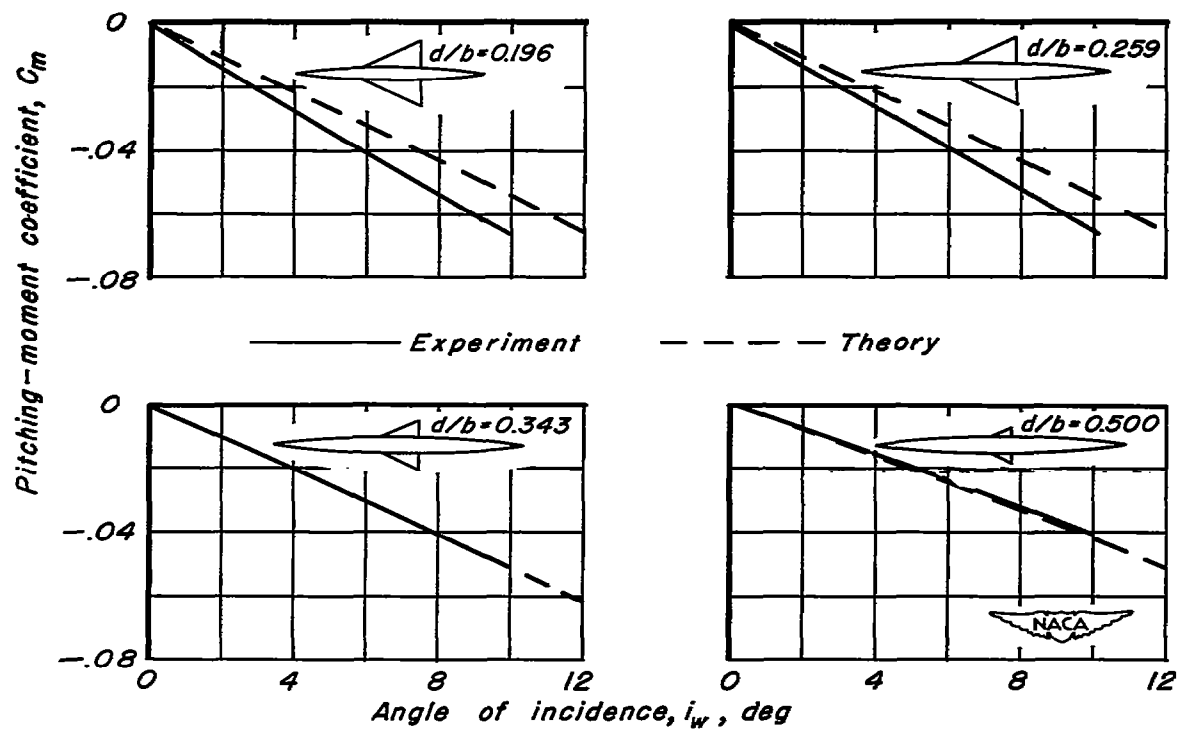
(e) C_m vs i_w, $\alpha = 0°$

Figure 5.— Continued.
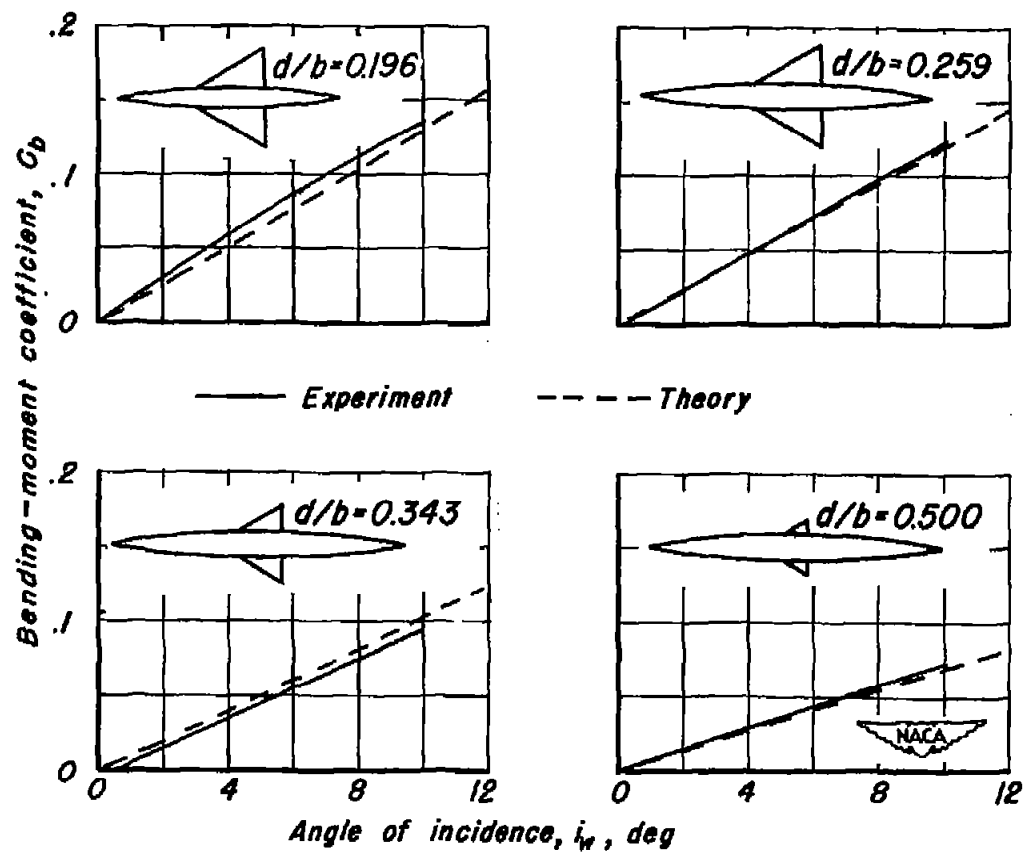
(f) C_b vs i_w, $\alpha = 0°$

Figure 5.— Concluded.

(a) α variable, $i_w = 0°$ (b) i_w variable, $\alpha = 0°$
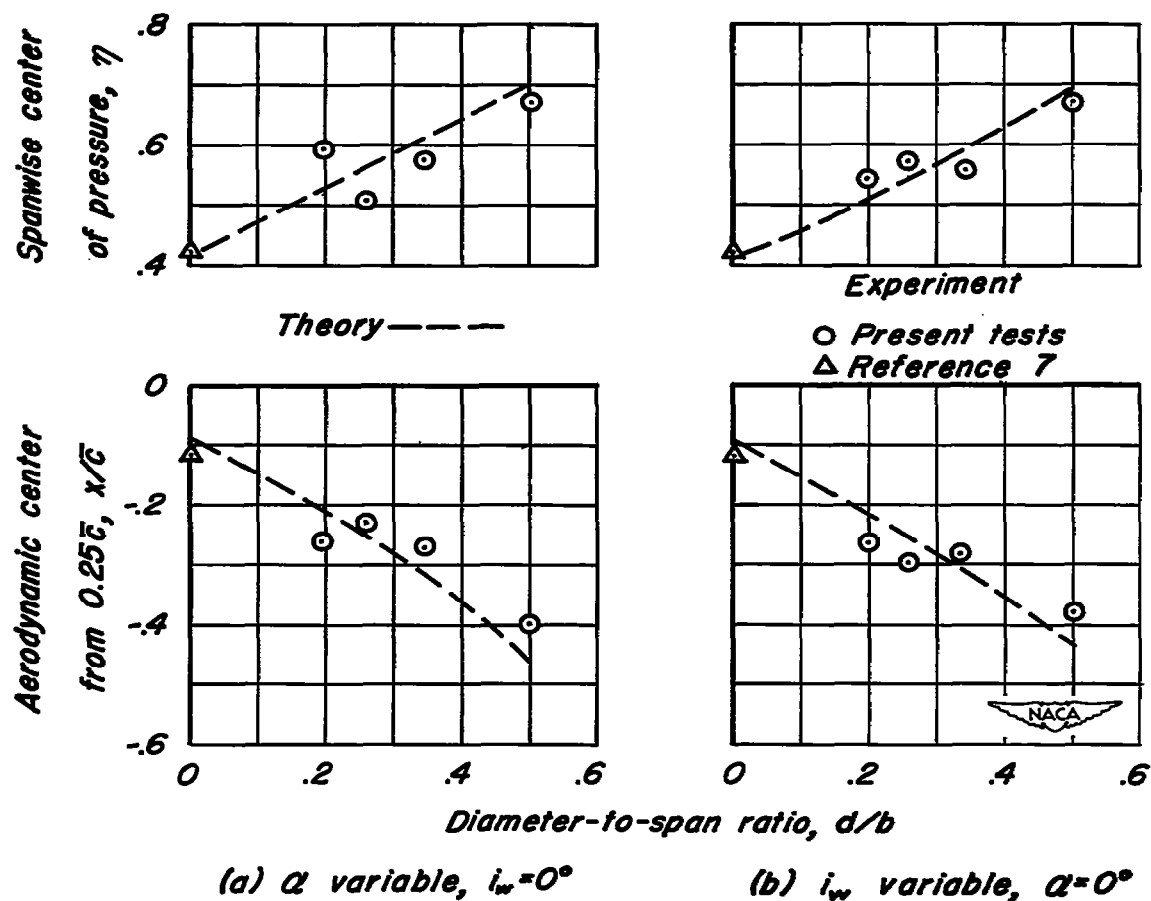
Figure 6.- Comparison between experimental and theoretical aerodynamic-center and spanwise center-of-pressure locations for the wings in the presence of the bodies.

—⊙— Experiment   ———— Lennertz's theory

$$\left[\frac{(dC_N/di_w)_{wing\ +\ body}}{(dC_N/di_w)_{wing\ in\ presence\ of\ body}}\right]_{\alpha=0^{\circ}} \qquad \left[\frac{(dC_N/d\alpha)_{wing\ +\ infinite\ cylinder}}{(dC_N/d\alpha)_{wing\ in\ presence\ of\ infinite\ cylinder}}\right]_{i_w=0^{\circ}}$$
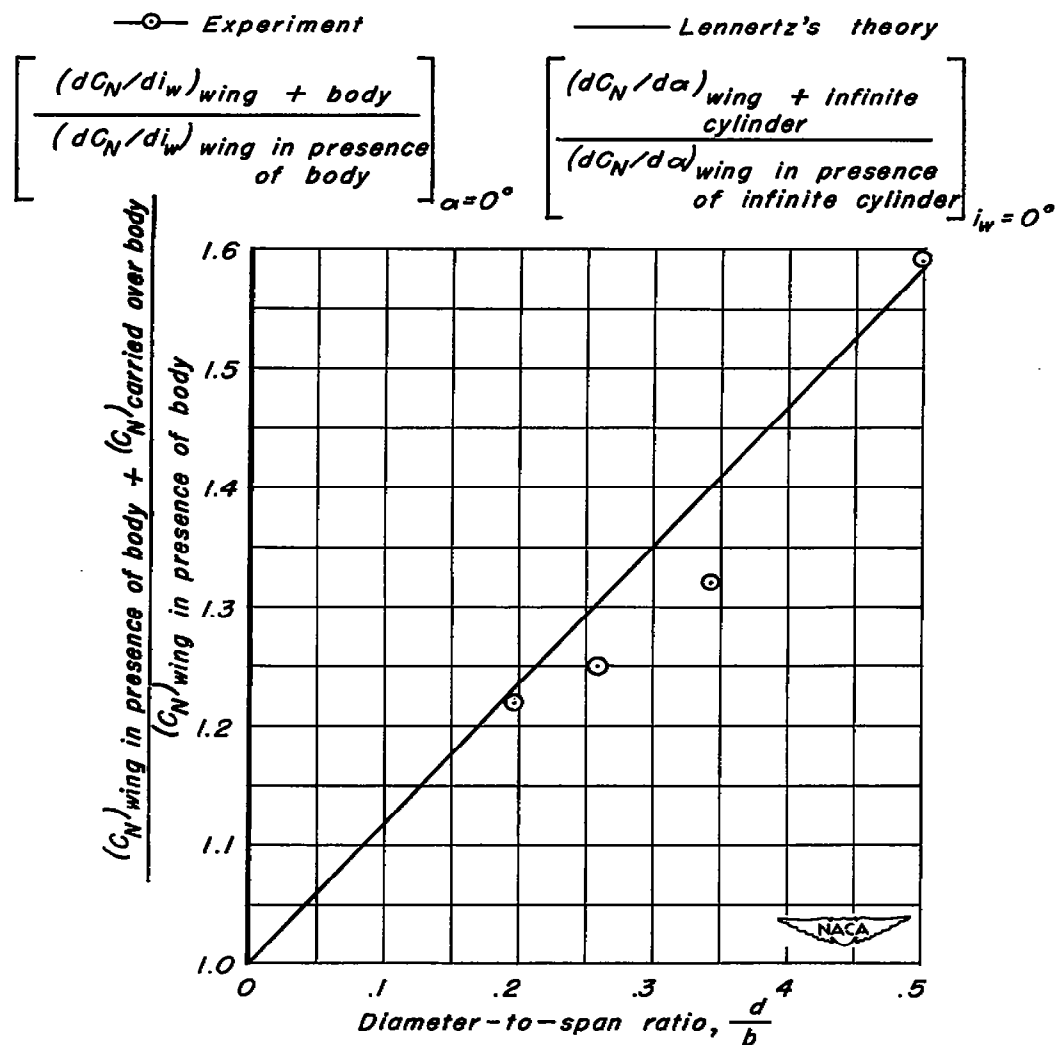
Figure 7.— Effect of diameter—to—span ratio on the amount of normal-
force coefficient carried over the bodies.
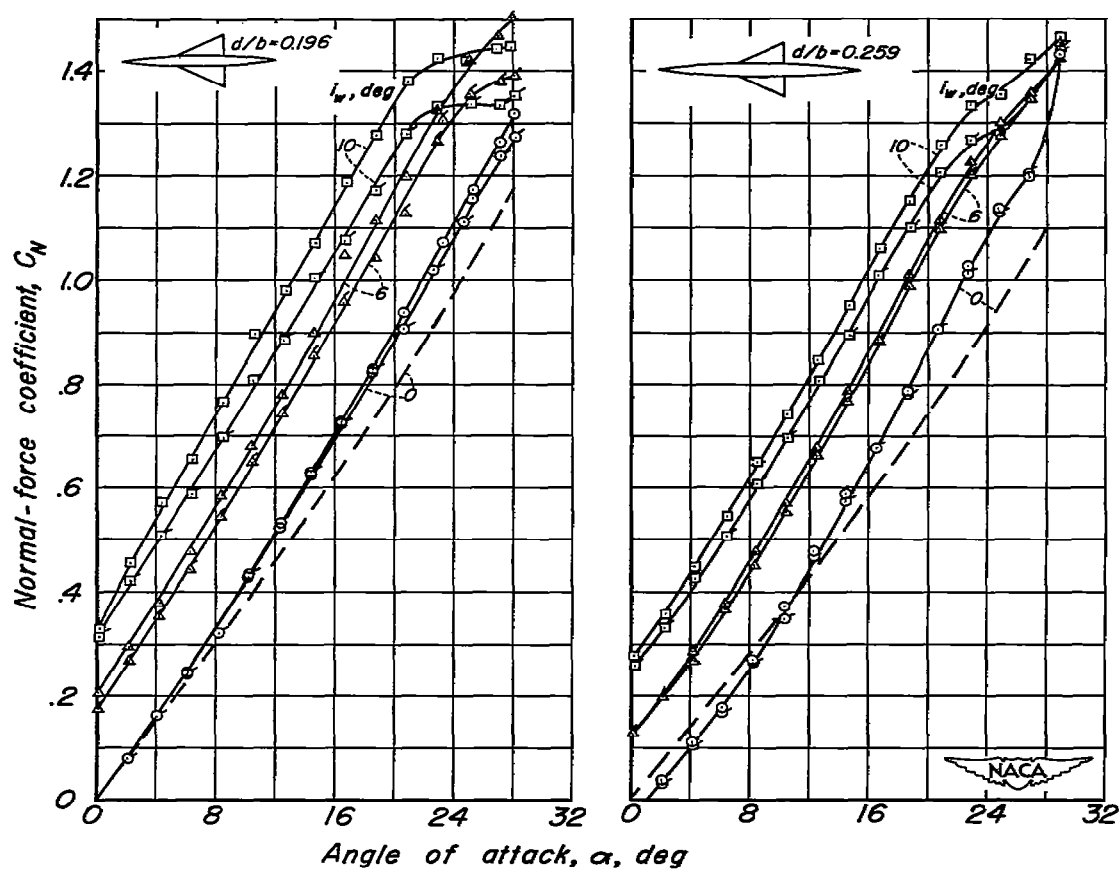
(a) C_N vs α, $\frac{d}{b}$ = 0.196 & 0.259

Figure 8.—Comparison between experimental and theoretical aerodynamic characteristics of the wing—body combinations.

RESTRICTED
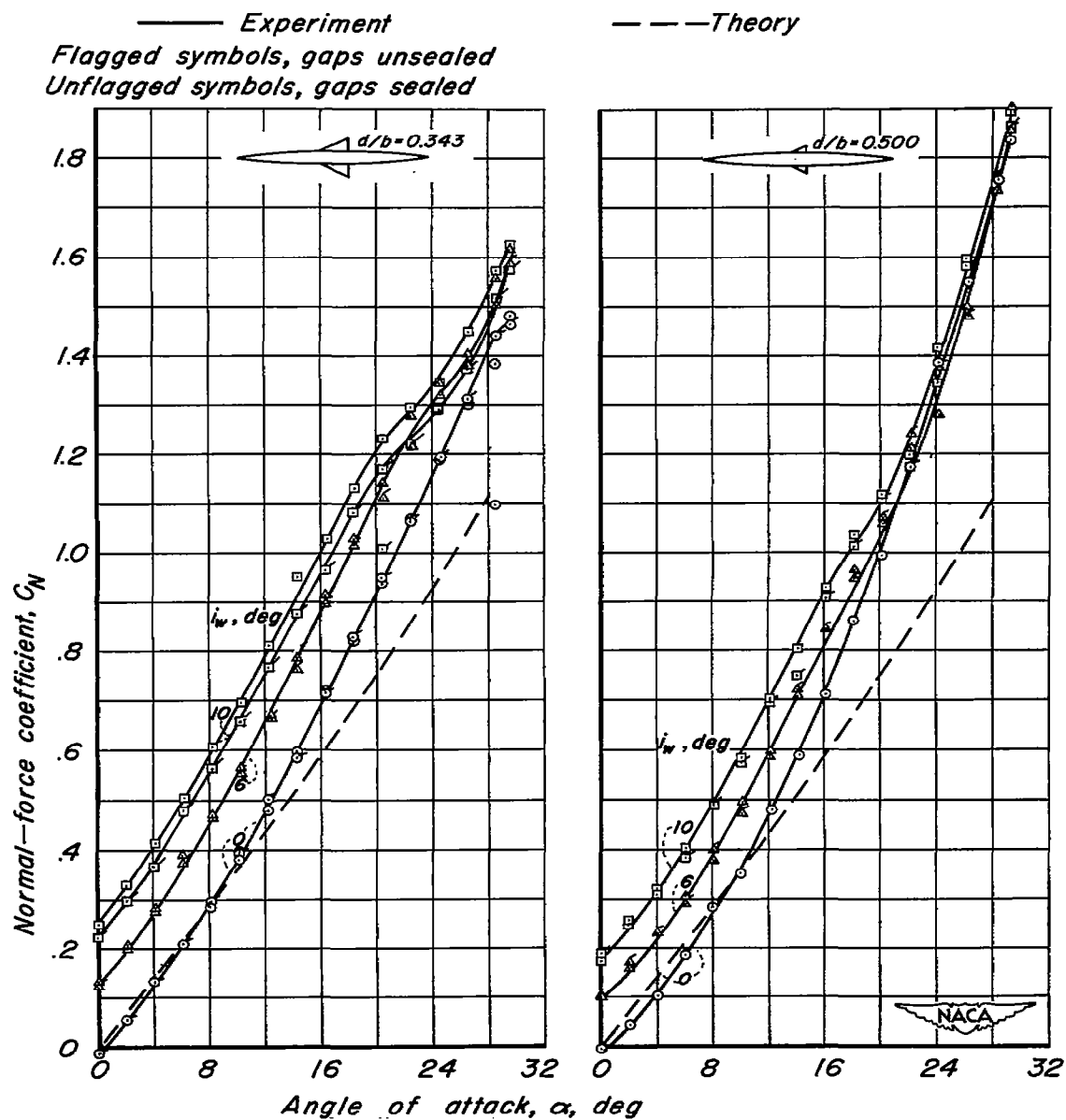
(b) C_N vs α, $\frac{d}{b} = 0.343$ & 0.500

Figure 8.—Continued.
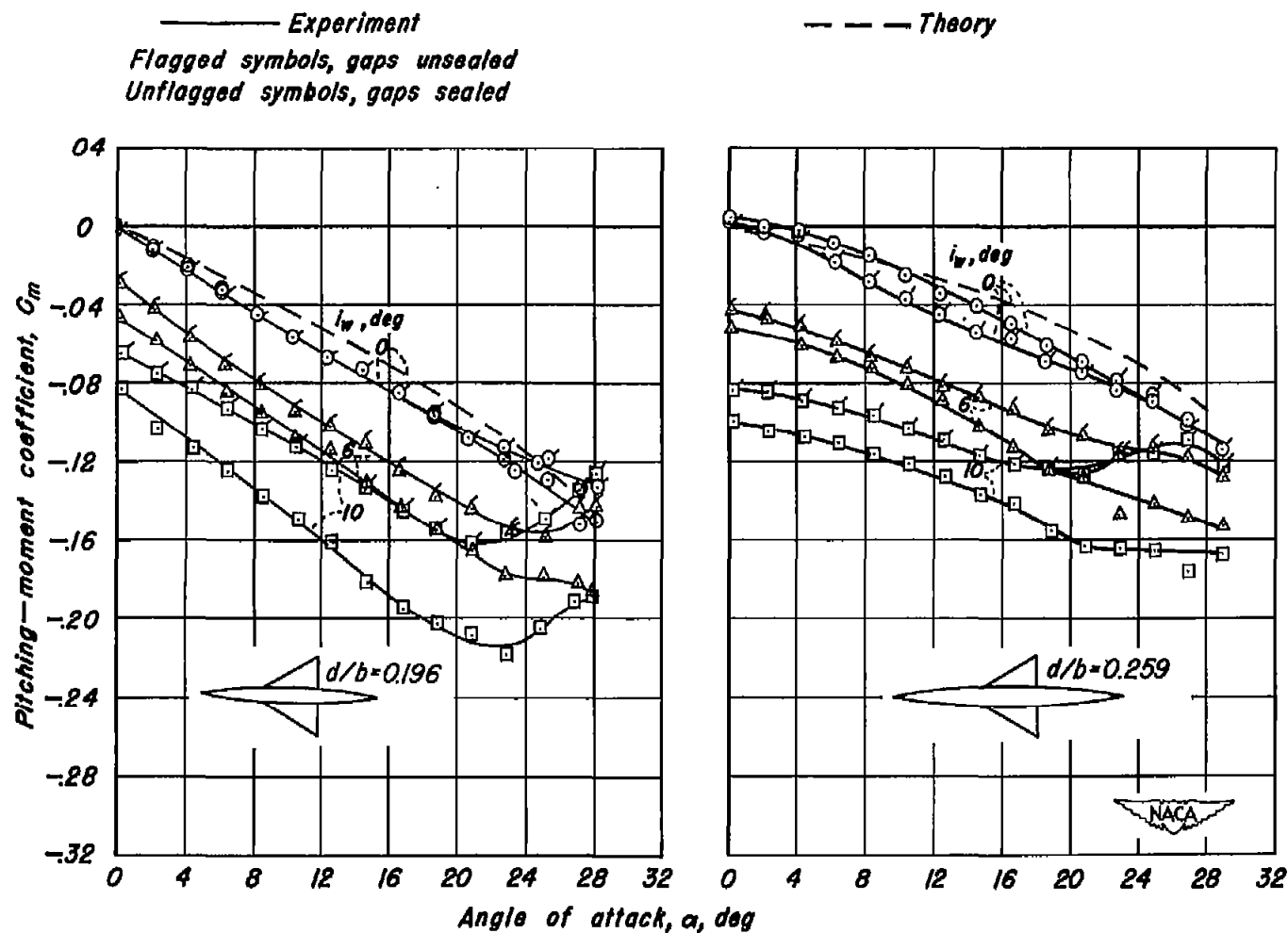
(c) C_m vs α, $\dfrac{d}{b} = 0.196$ & 0.259

Figure 8.—Continued.
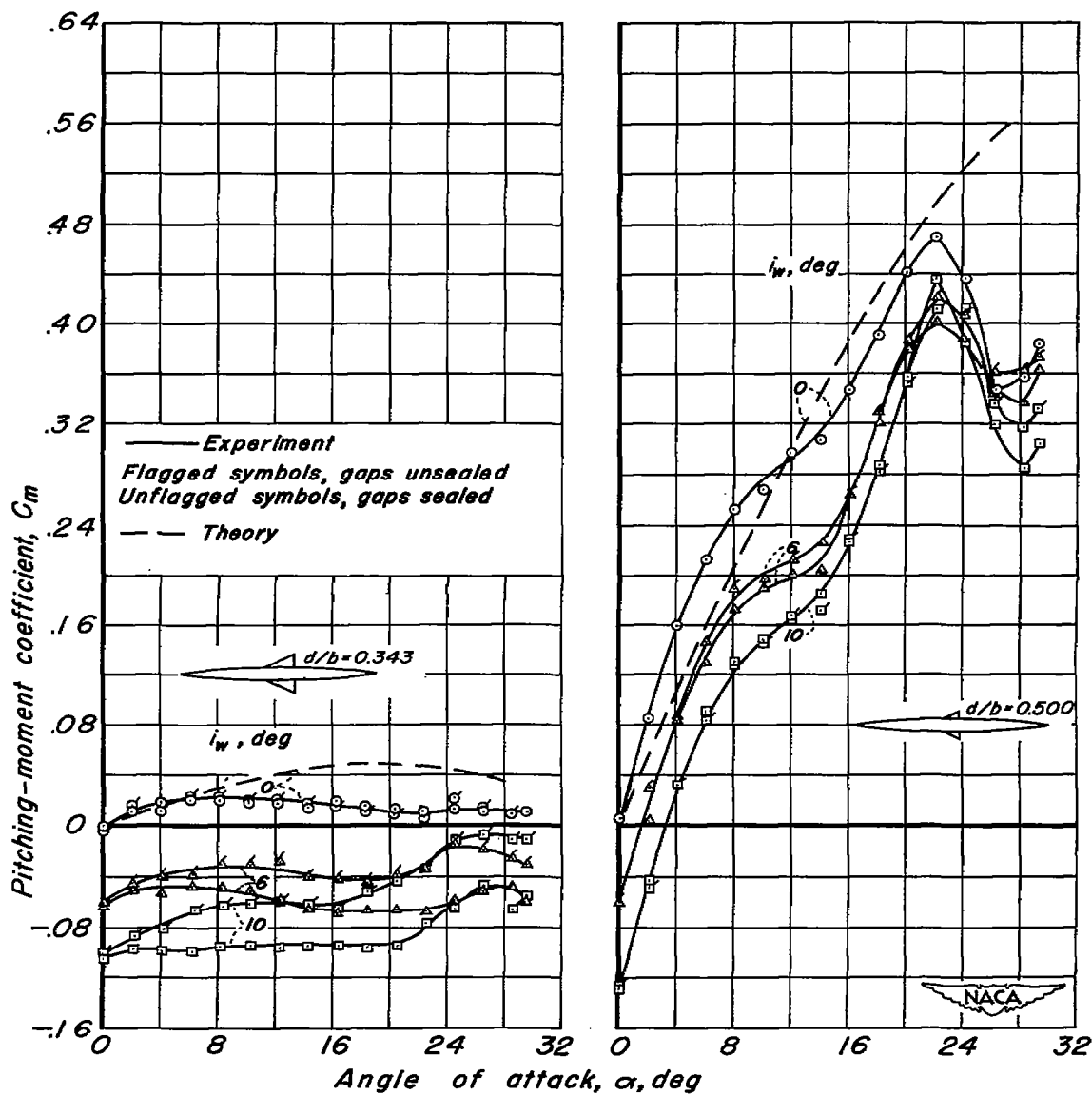
(d) C_m vs α, $\frac{d}{b} = 0.343$ & 0.500
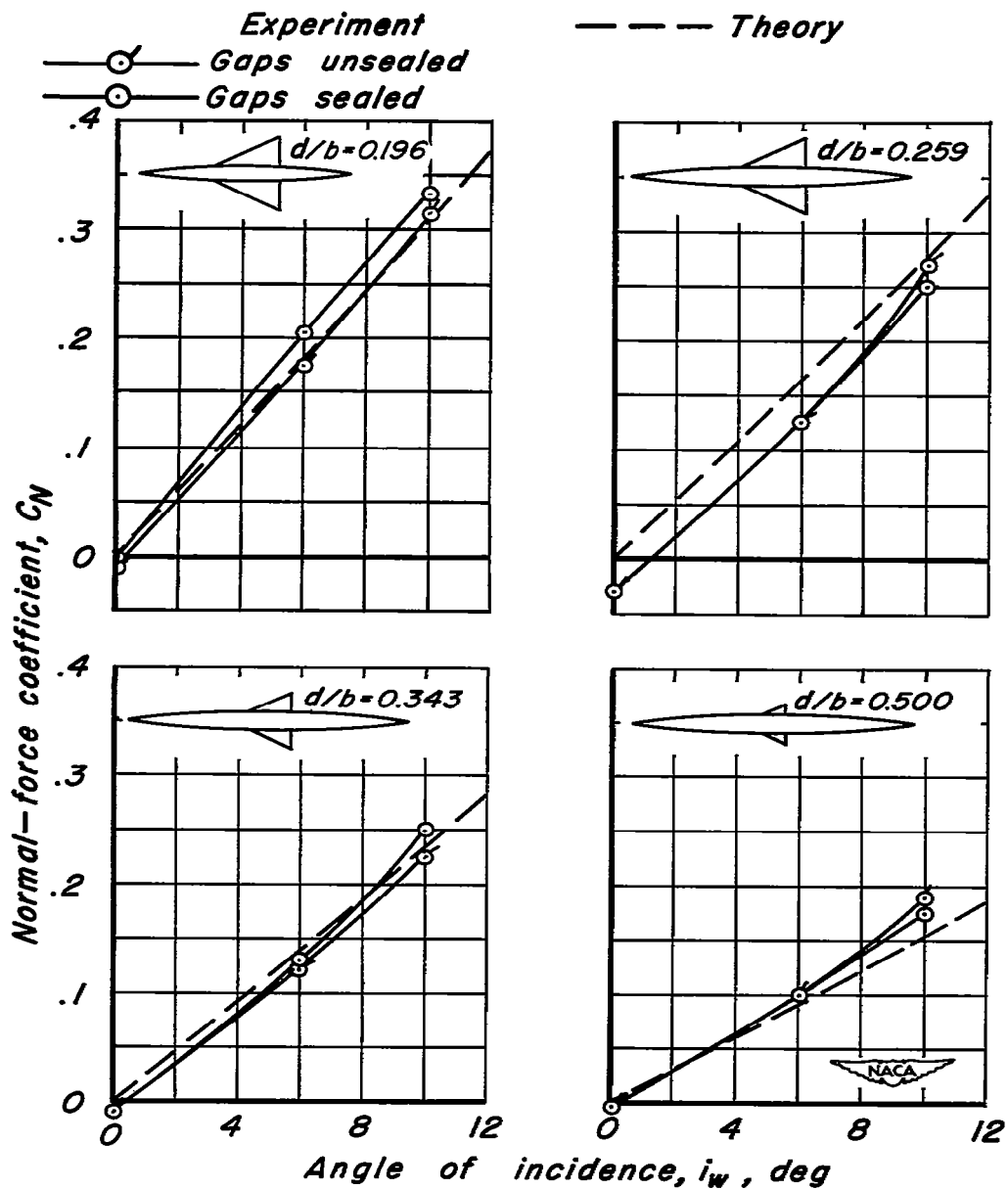
Figure 8.— Continued.

(e) C_N vs i_w, $\alpha = 0°$

Figure 8.— Continued.
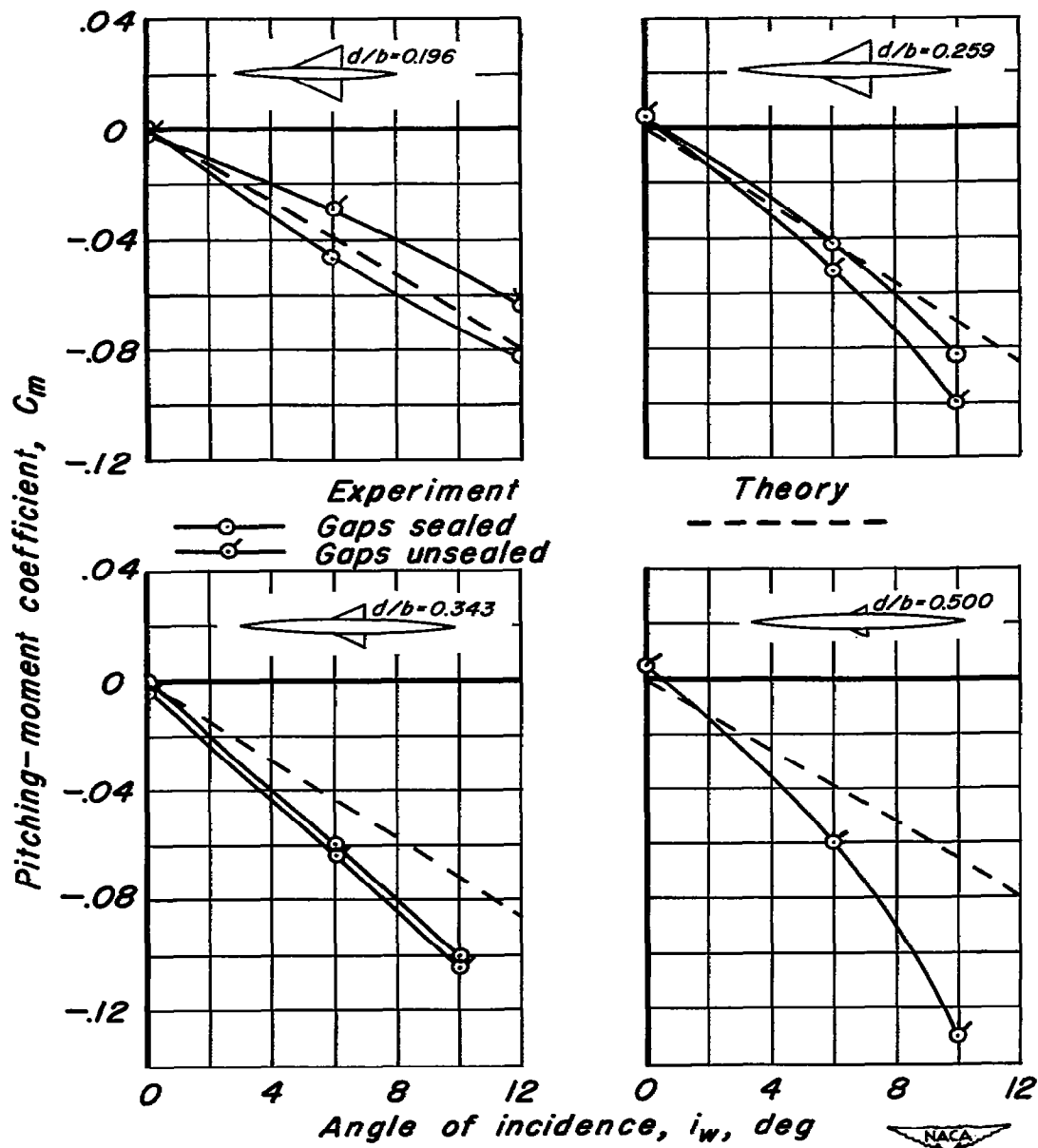
(f) C_m vs i_w, $\alpha = 0°$

Figure 8.—Concluded.

(a) α variable, $i_w = 0°$.   (b) i_w variable, $\alpha = 0°$.
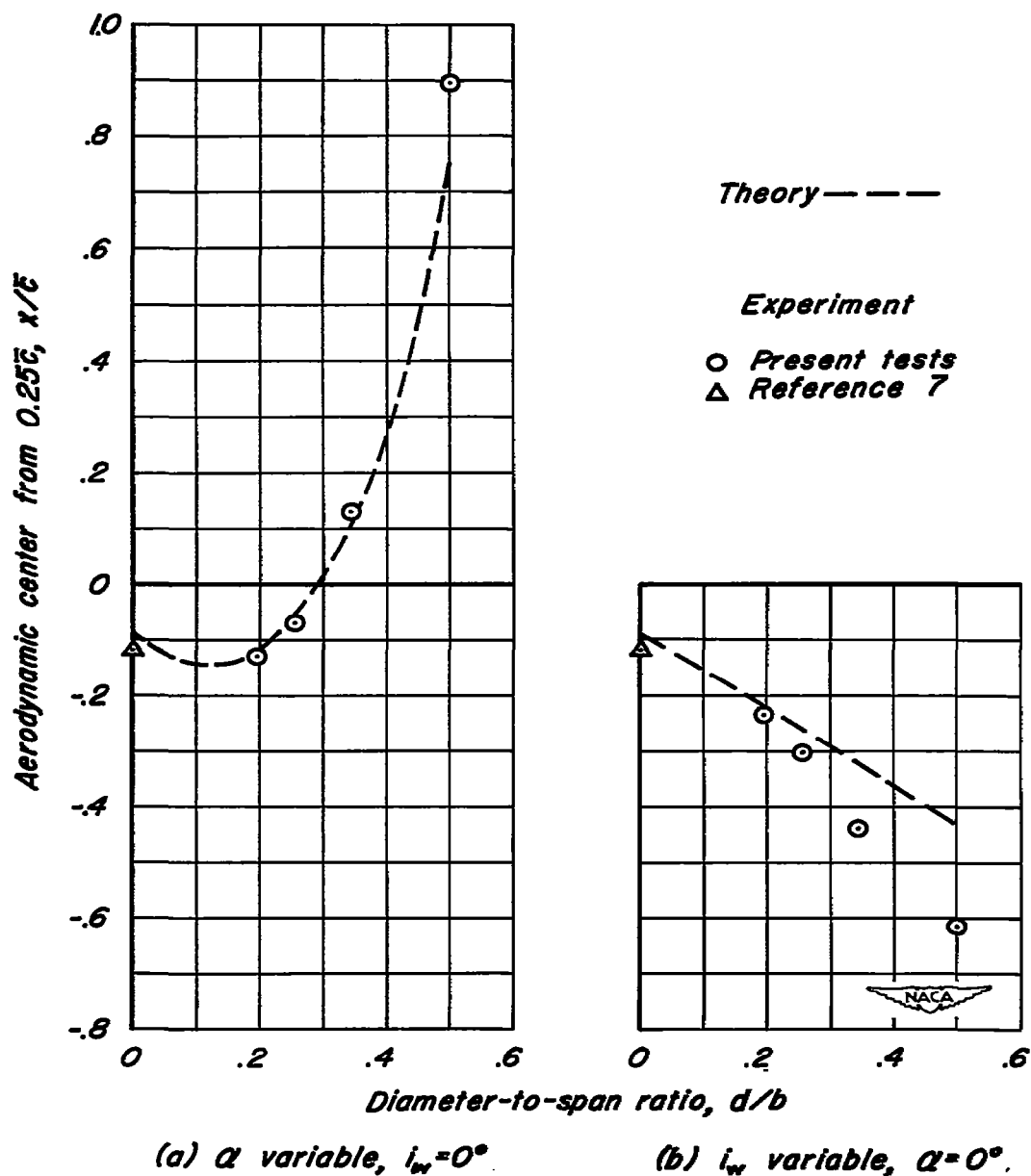
Figure 9.- Comparison between experimental and theoretical aerodynamic-center locations for the wing-body combinations.
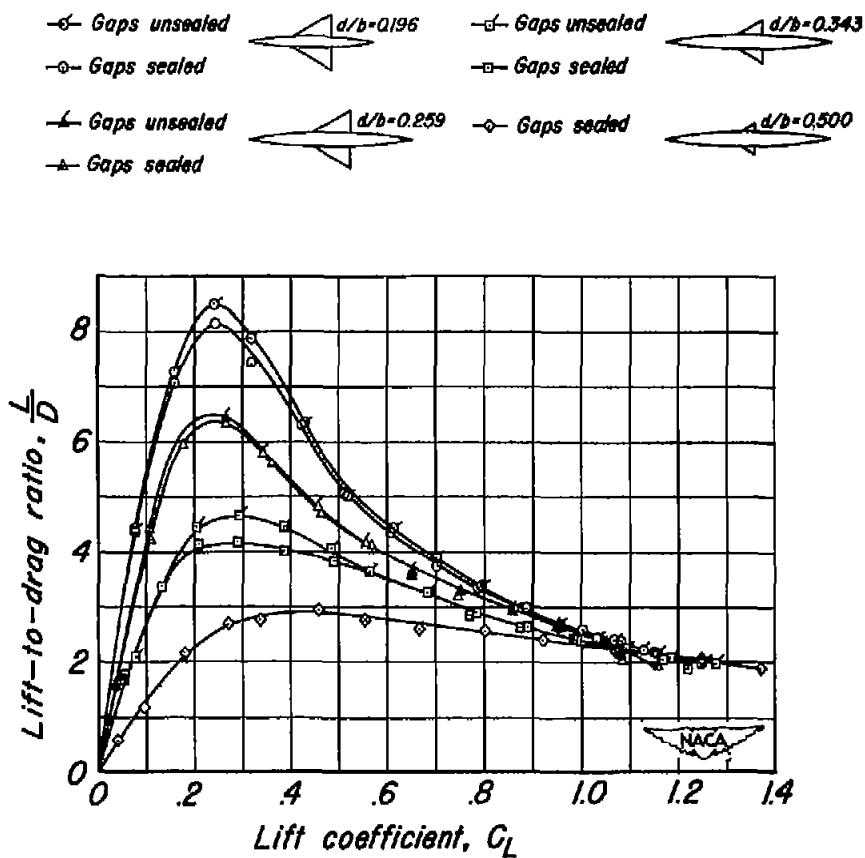
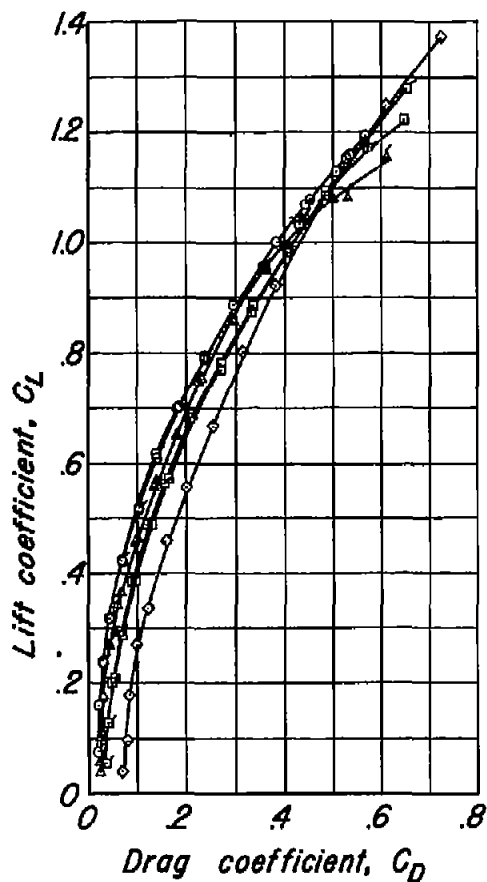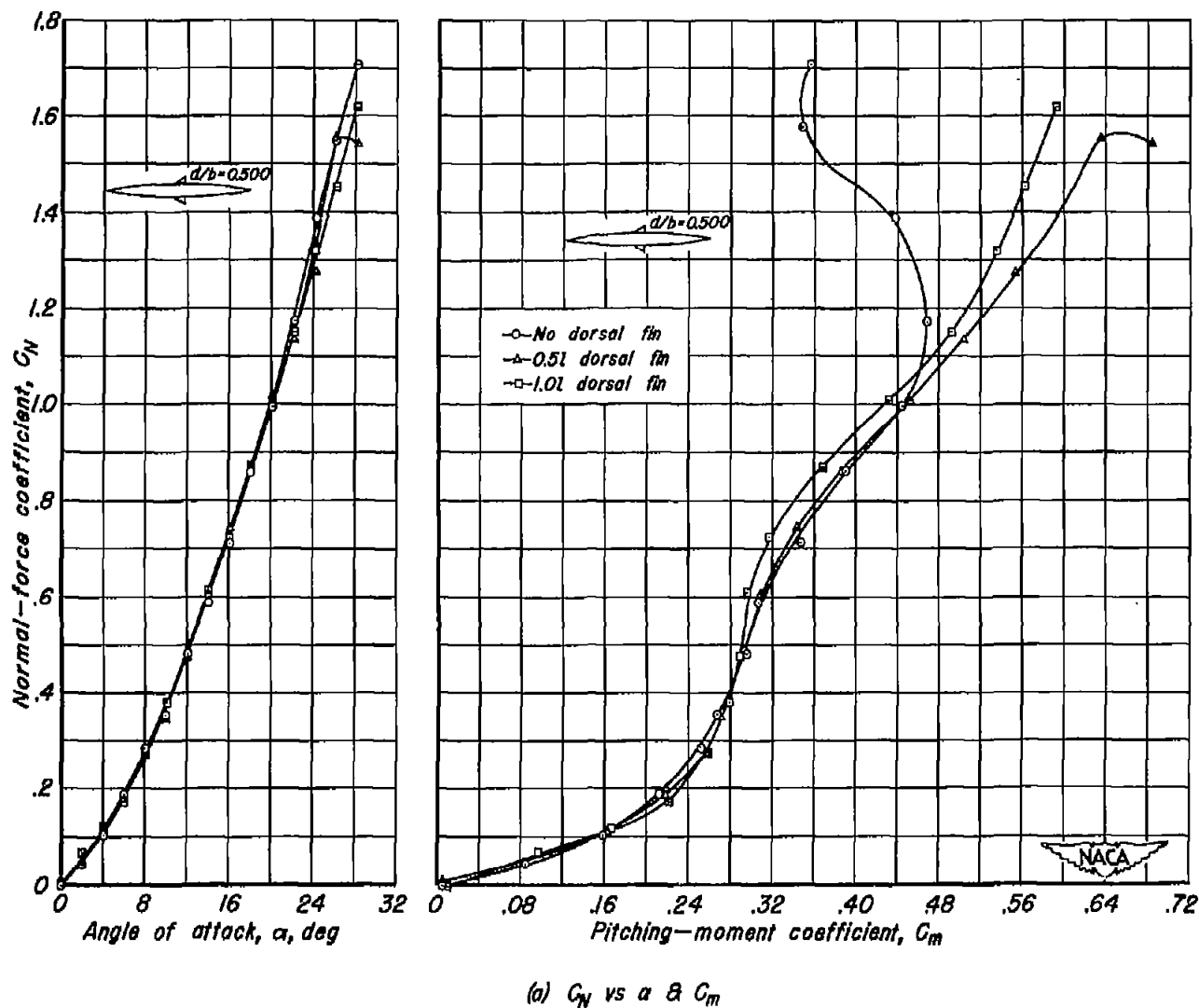Figure 10.— Drag characteristics of the wing-body combinations ($i_w = 0°$).

(a) C_N vs a & C_m

Figure 11.-Effect of dorsal fins on the aerodynamic characteristics of the wing-body combination with $\frac{d}{b}=0.5$.

d/b=0.500

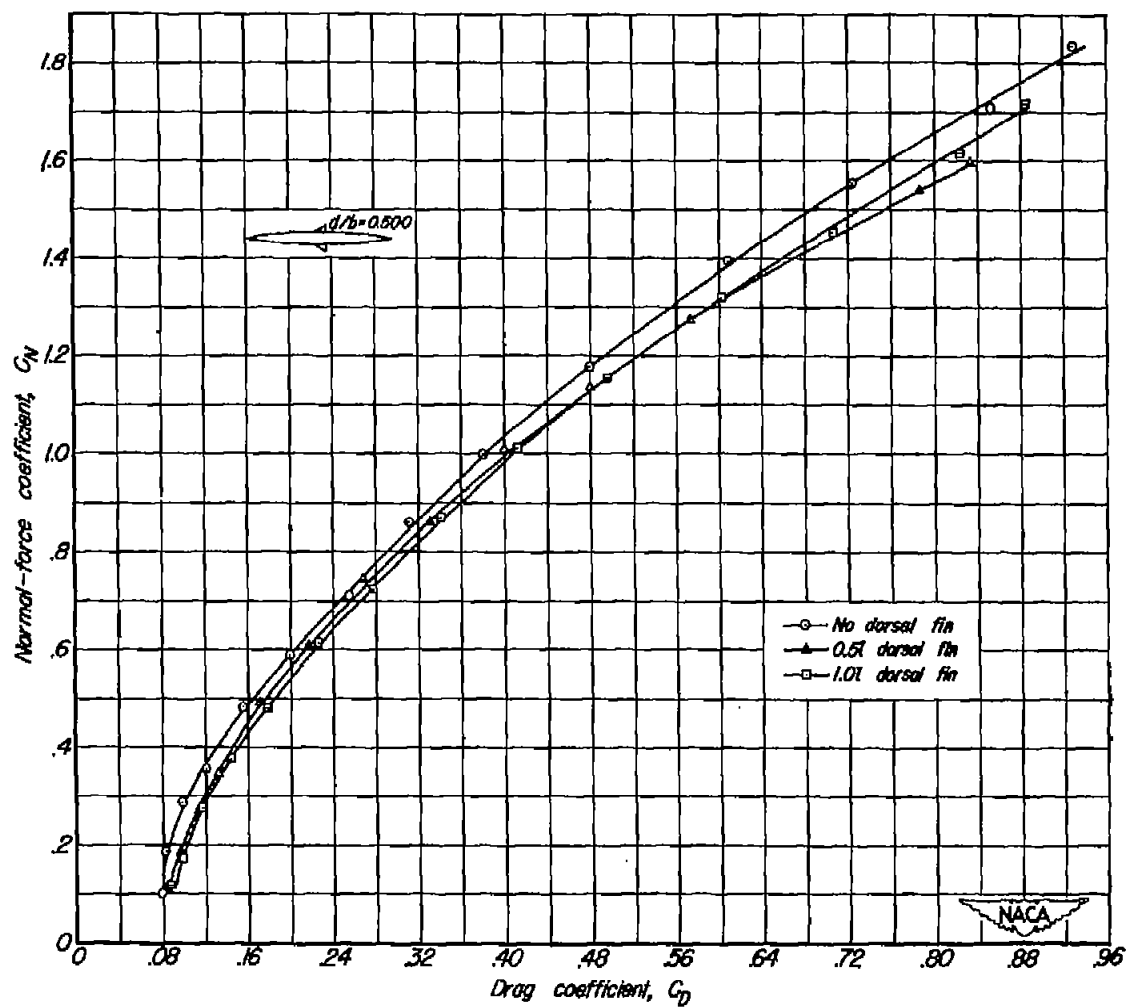—○— No dorsal fin
—▲— 0.5l dorsal fin
—□— 1.0l dorsal fin

(b) C_N vs C_D

Figure 11.—Concluded.